A 32-km Moist Primitive Equation Model Providing for Scale Interaction

MICHAEL L. KAPLAN[1]

Air Force Global Weather Central, Omaha, Nebr.

AND DOUGLAS A. PAINE

Division of Atmospheric Sciences, Cornell University, Ithaca, N. Y. 14850

(Manuscript received 22 May 1972, in revised form 16 October 1972)

ABSTRACT

A numerical model has been developed in an effort to simulate the interaction between quasi-geostrophic and mesoscale forcing. Initializations performed at 127 km with either a diagnostic omega equation or barotropic forecast are followed by a prediction with a moist nine-level primitive equation model at 32 km. Several integrations are performed utilizing both real and artificial data for the problem of the water-induced heat island in the cold season. The results of these integrations indicate important variations in both the patterns and intensity of development as a function of initialization.

1. Introduction

A numerical prognostic model has been developed in an effort to simulate the contribution of forcing functions at several scales of motion to an intense mesoscale development. The degree to which one can evaluate a weather modification experiment, for example, is highly correlated with the nature of the synoptic and mesoscale boundary conditions. The numerical model to be discussed combines a transient synoptic-scale feature with horizontally varying low-level boundary conditions as well as detailed moist physical processes.

2. Physical model and equations

The physical model consists of two states: an initial and a prognostic state. Both real and artificial initial conditions are used. The real initial state is simulated by either an integration of a ten-level quasi-geostrophic omega equation or a single-level barotropic forecast, both of which are performed on a 127-km grid interval network shown in Fig. 1a. The solution of the diagnostic omega equation

$$\left(\nabla^2+\frac{f^2}{\sigma}\frac{\partial^2}{\partial P^2}\right)\omega=-\frac{f}{\sigma}\frac{\partial}{\partial P}[-\mathbf{V}\cdot\nabla(\zeta+f)]+\frac{1}{\sigma}\nabla^2\left(-\mathbf{V}\cdot\nabla\frac{\partial\Phi}{\partial P}\right), \quad (1)$$

or the solution of a single-level barotropic forecast model

$$\nabla^2\frac{\partial Z}{\partial t}=-\tfrac{1}{4}[J(Z,\zeta+f_0)], \quad (2)$$

provides an initial set of dependent variables at the 127-km grid. (Appendix A contains a list of mathematical symbols.) From either quasi-geostrophic model the appropriate assumptions may be made which allow for a complete set of dependent variables at nine atmospheric levels. Once this initialization is performed, there exists a first approximation to the fluid flow at the synoptic scale. We may also perform an artificial initialization if it is assumed that a horizontal and vertical stratification of temperature and geopotential height exist. The u and v horizontal wind components are derived from the geostrophic wind law, while values of the vertical velocity and moisture distribution are assumed. The dependent variables developed for the synoptic-scale 127-km grid may be interpolated to a 32-km grid network shown in Fig. 1b to serve as the initial dependent variables for a mesoscale prognostic primitive equation (P.E.) model.

The 32-km P.E. model has nine vertical levels illustrated in Fig. 2, i.e., 50 m above the planetary surface, and 950, 875, 800, 700, 600, 500, 300 and 100 mb. The zone between 950 mb and the lowest level is assumed to be a well-mixed fluid, where turbulent overturning is simulated via bulk aerodynamic expressions. The lifting condensation level and the top of the Ekman layer are both put at 875 mb.

The time-dependent equations relate total water substance (Q), temperature (T), horizontal velocity components (u, v), and surface pressure (P_s). The

[1] Previous affiliation: Department of Atmospheric Science, State University of New York at Albany.

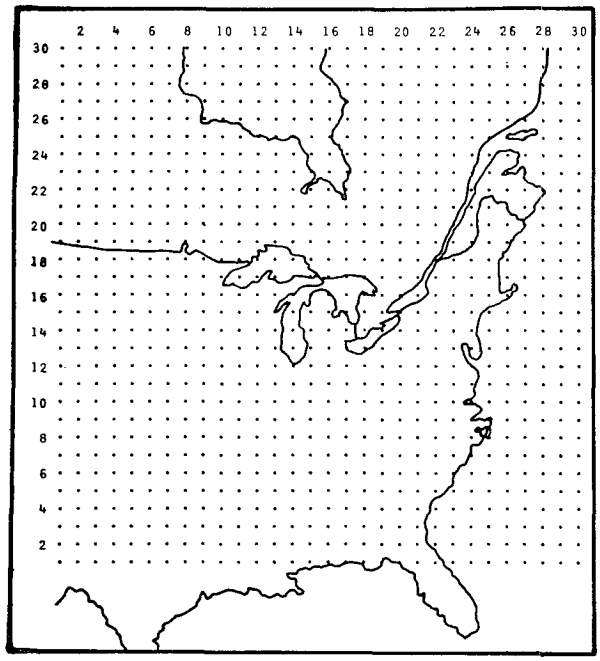

FIG. 1a. 127-km grid mesh for determining quasi-geostrophic forcing.

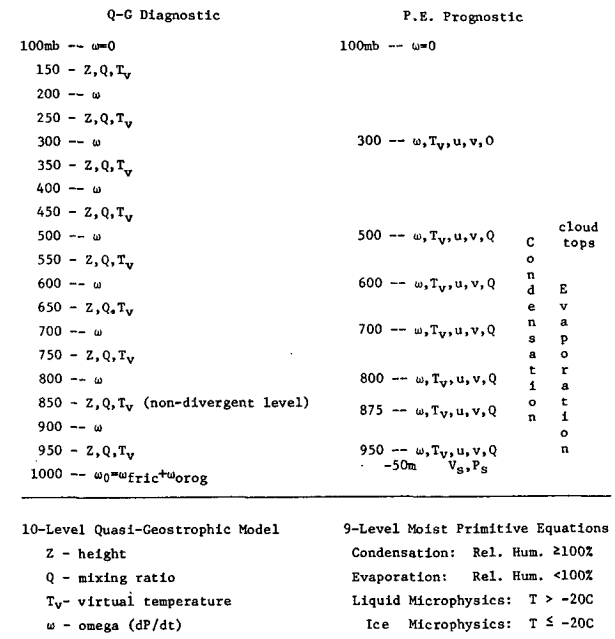

FIG. 2. Vertical resolution and the dependent variables of the diagnostic and prognostic models.

diagnostic relationships include the virtual temperature, geopotential height, and kinematic omega equations. The total moisture substance equation is

$$\frac{\partial Q}{\partial t}=-m(\mathbf{V}\cdot\nabla Q)-\omega\frac{\partial Q}{\partial P}-C_1+C_2, \tag{3}$$

where C_1 and C_2 are the low-level moisture flux and condensation functions, respectively. Term C_1 is applied only at 950 mb with the term $-\omega(\partial Q/\partial P)$ applied at all other model levels. The expression for the flux of heat and moisture is similar to that used by Lavoie (1968). However, in this model an average value of the flux term is used incorporating stresses at the 950- and 875-mb surfaces. Condensation is allowed in the model at 875, 800, 700, 600 and 500 mb, while evaporation is allowed at 950–600 mb. Condensate is developed when the relative humidity exceeds 100%. Evaporation is allowed at the aforementioned levels when a level is undersaturated and the level directly above it is supersaturated. The storage of water substance is a function of temperature and pre-existing water substance at any level:

$$\text{storage}=Q-\{[(268.16-T)0.02]+0.1+[(Q-Q_{\text{sat}})^{10}]\}. \tag{4}$$

This relationship assumes a precipitation efficiency of 10% for temperatures above −5C, with a linear increase to 50% maximum at −25C. The second factor in the above relationship is a crude estimate of collision-coalescence processes which assumes an additional 10% of the water substance is released. All model physical processes are assumed with respect to ice at temperatures $\leqslant -20$C, and with respect to water above this value. Condensate is allowed to drop at the rate of one model level per time step. In precipitation calculations, cloud depths are a function of the vertical extent of consistent ascent. Snowfall-to-meltwater ratios are assumed to be 15:1 (Jiusto and Kaplan, 1972). The storage term is included in term C_2 of Eq. (3) by augmenting the

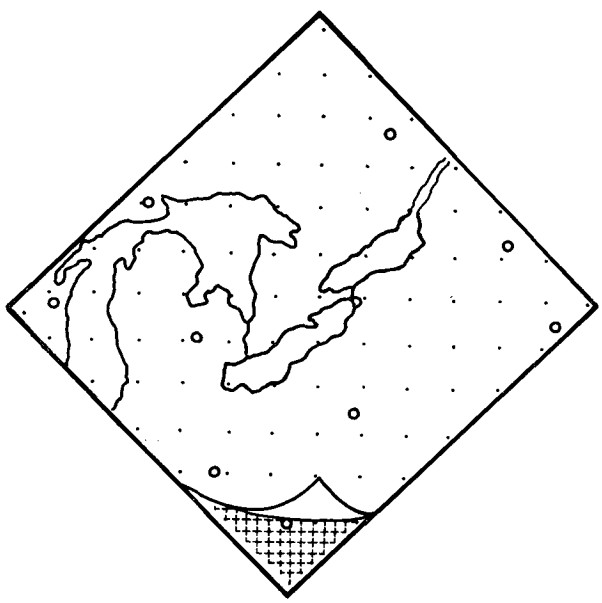

FIG. 1b. 32-km mesoscale grid (cross marks) and area of integration of the primitive equation model.

amount of water substance released in the condensation process.

The temperature prognostic equation is

$$\frac{\partial T}{\partial t}=-m(\mathbf{V}\cdot\nabla T)-\omega\left(\frac{\partial T}{\partial p}-\frac{\alpha}{C_p}\right)-H_1+H_2, \tag{5}$$

where H_1 and H_2 are the low-level turbulent flux of heat and latent heating, respectively; H_1 is applied only at 950 mb, while the adiabatic cooling term $-\omega[(\partial T/\partial p)-(\alpha/C_p)]$ is applied above 950 mb. The latent heating term is expressed as $(L/C_{pm})\Delta c$, with Δc equalling the mass of condensate or evaporate (negative condensate) per time step.

The equations of motion are

$$\frac{\partial u}{\partial t}=-m(\mathbf{V}\cdot\nabla u)-\omega\frac{\partial u}{\partial P}+fv-m\frac{\partial \Phi}{\partial x}+F_x, \tag{6}$$

$$\frac{\partial v}{\partial t}=-m(\mathbf{V}\cdot\nabla v)-\omega\frac{\partial v}{\partial P}-fu-m\frac{\partial \Phi}{\partial y}+F_y, \tag{7}$$

where F_x and F_y are the frictional forces calculated by integrating the stress between the surface and the 950- and 875-mb levels.

The final time-dependent equation for the pressure tendency is

$$\frac{\partial P_s}{\partial t}=-m(\mathbf{V}_s\cdot\nabla P_s)+w\frac{\partial P}{\partial Z}+\int_{P_{950}}^{P_{300}}\nabla\cdot\mathbf{V}\partial p, \tag{8}$$

where the last two terms are the orographically-induced omega and the integral of the divergence, i.e., the kinematic omega equation solved using the trapezoidal rule. This omega equation is simply the equation of continuity in the form

$$\frac{\partial \omega}{\partial p}=-m^2\nabla\cdot\mathbf{V}. \tag{9}$$

3. Numerical method

Since the prime purpose of the numerical experiment is to simulate the nonlinear interaction among scales of motion in the atmosphere, the damping characteristics of the numerical scheme are critical to the success of the problem. The Euler-backward scheme (Matsuno, 1966) is employed because of its highly selective damping characteristics. Gerrity and McPherson (1970) have shown that this scheme damps the 2Δ waves most effectively at numerical stability ratios of approximately 1. If it is assumed that $g\approx 10$ m sec^{-2}, $\Delta X\approx 32$ km, and a scale height of the disturbance $H\approx 3$ km, solution for the time step from the relationship for the stability ratio $(gH)^{\frac{1}{2}}(\Delta t/\Delta X)$ yields a $\Delta t\approx 185$ sec for neutral stability. This maximum damping of the 2Δ wave paralleling very weak damping of the quasi-geostrophic wave allows the initial transient synoptic-scale feature to alter (or be altered) by smaller scale energy sources and sinks. The damping of the 2Δ wave is not restricted to the temporal mode; the spatial mode is also damped by applying a filter $\overline{u^{*xxyy}}$ ($u^*=\frac{1}{2}u^n$) for both components of the velocity field (McPherson, 1971). Thus, the quasi-geostrophic and mixed Rossby-gravity wave systems are allowed in the numerical solutions while restricting the 2Δ higher frequency gravitational modes.

The Euler-backward scheme consists of a guess and then a correction to this guess, i.e.,

$$\left.\begin{aligned}\epsilon^{*\tau+1}-\epsilon^{\tau}&=f(\epsilon^{\tau})\Delta t\\ \epsilon^{\tau+1}-\epsilon^{\tau}&=f(\epsilon^{*\tau+1})\Delta t\end{aligned}\right\},$$

where ϵ is any dependent variable, and asterisks refer to first-guess values. This process tends to reduce the higher order solutions relative to the first- and second-order parts of the series.

The lateral boundary conditions for the u, v, Q, T equations assume a spatial averaging of adjacent points for outflow boundaries as described by Nitta (1962). The inflow boundaries are set equal to the first interior point for each time step for dependent variables u,v,Q,T. Both inflow and outflow boundaries for P_s are assumed to be zero.

4. Results of numerical integrations

Four integrations were performed by the P.E. model with different initializations. All four integrations had two elongated lakes surrounded by colder land areas as low-level boundary conditions. These warm water bodies were designed to simulate Lakes Erie and Ontario. The mesoscale grid consisting of nine vertical levels of a 36×32 horizontal matrix was centered over both lakes, with $\sim$32 km separating each grid point.

In all but one of the initializations the lakes were assumed to be 10C warmer than the overlying atmosphere. The value of mixing ratio at the water surface was assumed to be 90% of the saturation mixing ratio at the lake temperature ($\sim$50F). The values of drag coefficient were assumed to vary from 0.40 over land to 0.0016 over water (Lavoie, 1968). The surface u and v wind components were approximated as being 67% of the 950-mb values.

Two of the four integrations were performed with "real" initial data from the quasi-geostrophic models, where "real" designates an approximation toward the actual synoptic-scale state of the atmosphere. The initial synoptic situation has been described in detail by Paine (1971) and Paine and Kaplan (1971). At 1800 GMT 4 November 1967, a weak trough with a wavelength of $\sim$1000 km is about 200 n mi west of Lakes Erie and Ontario (Fig. 3). Positive vorticity advection at low levels is approaching both lakes. It is this quasi-geostrophic organization which helps provide

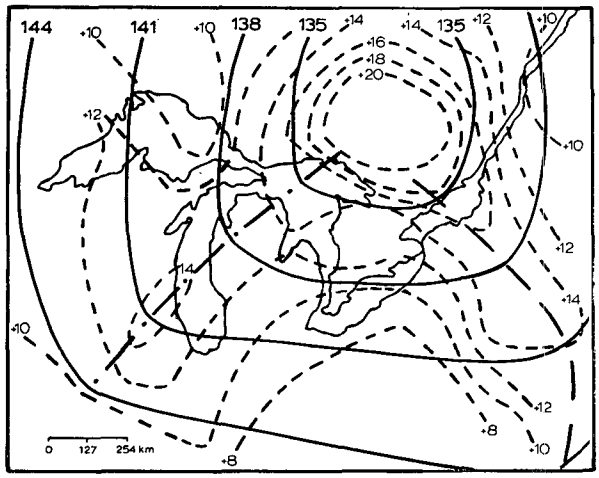

FIG. 3a. 850-mb forecast height (dkm) and absolute vorticity ($\times 10^{-5}$sec^{-1}) for 1800 GMT 4 November 1967.

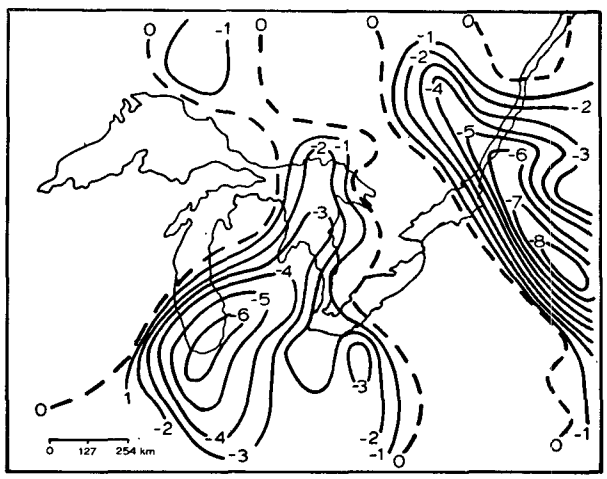

FIG. 3b. 850-mb forecast ascent (μb sec^{-1}) on the 127-km grid for 1800 GMT 4 November 1967.

a favorable environment for low-level heat, moisture, and momentum flux, plus vigorous latent heating.

a. Integrations with no synoptic influence

To test the importance of this synoptic feature in organizing the release of energy at smaller scales, we at first ignore the presence of the trough by assigning no initial Laplacian of geopotential heights. That is, the first two integrations using artificial initial fields begin with a constant horizontal variation of temperature (and therefore, geopotential height), while permitting a slight increase in wind velocity with elevation. This initial zero value for $\nabla^2 Z$ assures that the model will have no initial omega and, consequently, no aid from the quasi-geostrophic scales in liberating energy stored at the mesoscale.

In one of the integrations the exact same low-level boundary conditions were utilized as in the real data initializations. In the other integration, the low-level lake temperature excess was 20C instead of 10C. The 20C case was integrated out to 5 hr of real time and the 10C case was integrated to 8 hr. The difference in the forecast fields is rather striking. The 8-hr integration with the 10C excess shows a maximum vertical motion of only $-0.6\,\mu$b sec^{-1} (Fig. 4a). The 950-mb temperature field shown in Fig. 4b has virtually no lake-induced thermal pattern.

The 5-hr 20C integration, however, shows rather vigorous development with omegas to $-10\,\mu$b sec^{-1} (Fig. 5a) and a strong 950-mb horizontal gradient of temperature due to lake-induced heat flux (Fig. 5b). There is, however, only minimal latent heating at 875 mb.

The startling difference between these two cases merely emphasizes the nonlinear nature of energy exchange in the geophysical fluid. Without an initial horizontal shear to stimulate the low-level turbulent fluxing terms (which are no more than merely parameterized non-hydrostatic transport or mixing processes),

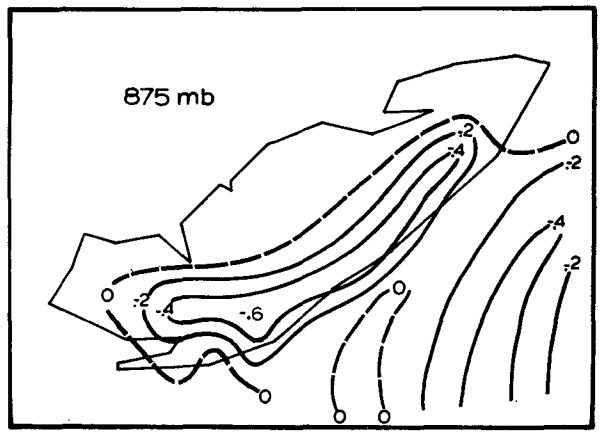

FIG. 4a. Forecast omega (μb sec^{-1}) after 150 time steps or 8 hr elapsed time, no initial omegas, and with a +10C lake temperature excess. Ascent only is shown.

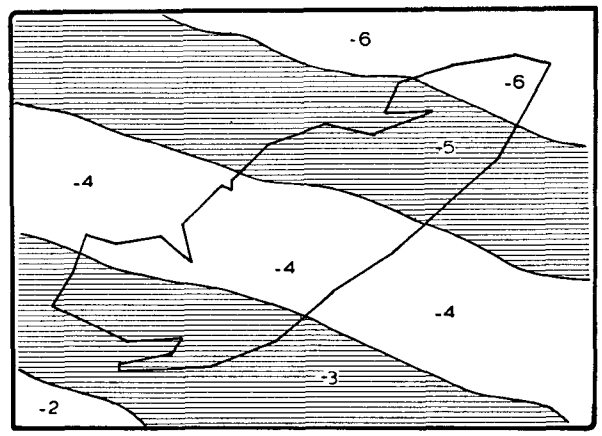

FIG. 4b. 950-mb forecast temperature after ~8 hr, no initial omegas, and with a +10C lake temperature excess.

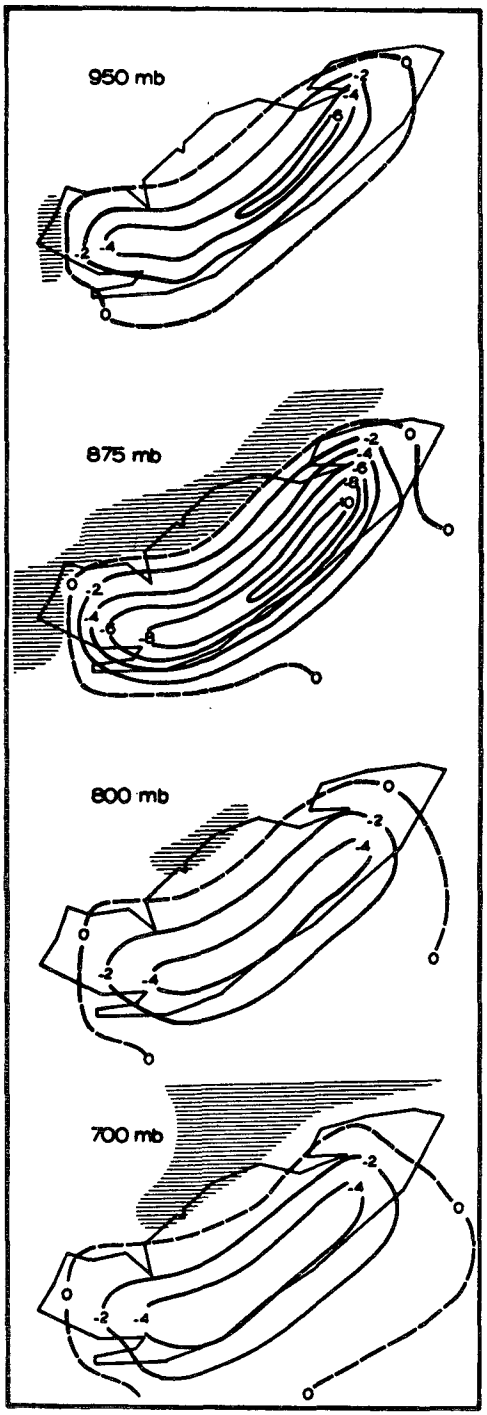

FIG. 5a. Forecast omega after 100 time steps or 5 hr elapsed time, with Lake Erie temperature excess = +20C. Shading represents descent ≥ 2 μb sec^{-1}.

the moderately strong 10C vertical gradient is not sufficient to warp the 950-mb surface. However, the stronger gradient represented by the initial 20C temperature excess is apparently capable of creating enough of an acceleration, shear and reinforcement of the low-

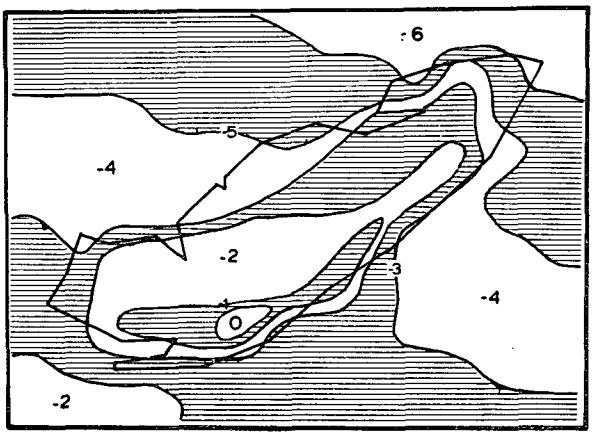

FIG. 5b. 950-mb forecast temperature after 5 hr, no initial omegas, and with a +20C lake temperature excess.

level mixing process to enhance the flux of energy in time. These results could lead one to conclude that without a strong vertical gradient of temperature, an initial distortion in the fluid flow pattern is a necessary ingredient in the process of development.

b. Barotropic approximation to the initial synoptic state

The equivalent barotropic model with initial data from 1200 GMT 4 November is utilized for a 6-hr forecast to 1800 GMT 4 November at 850 mb, i.e., the constant pressure surface near the non-divergent level of the low-level trough (Paine and Kaplan, 1971). The next integration is performed with the single-level, 127-km barotropic forecast initialization shown in Figs. 3a and 3b. Simple linear assumptions concerning the vertical variation of temperature (and hence, geopotential) are used to extrapolate dependent variables to all P.E. model levels. Additional omegas are computed by integrating the equation of continuity. Likewise, the values of Q are extrapolated through the vertical and horizontal using approximations based on the 10 initial soundings taken within the 32-km grid area.

A 6-hr integration is performed with the nine-level P.E. model out to 0000 GMT 5 November 1967, using this highly simplified barotropic initialization. Although the results of these integrations are described in greater detail by Kaplan and Paine (1972), the mesoscale forecast potential of this method of initialization may be seen by comparing Figs. 6a and 6b. The maximum omega is forecast to be -25 μb sec^{-1} centered over Lake Erie at 875 mb (Fig. 6a). Substantial forecast ascent also extends into western Pennsylvania and over western Lake Ontario.

The vertical motion pattern may be seen to contain four to six delta gravity wave features, representing a link between the energy released at individual grid points[2] and the larger quasi-geostrophic wave. To show

[2] A cumulus parameterization scheme is outlined in Appendix B.

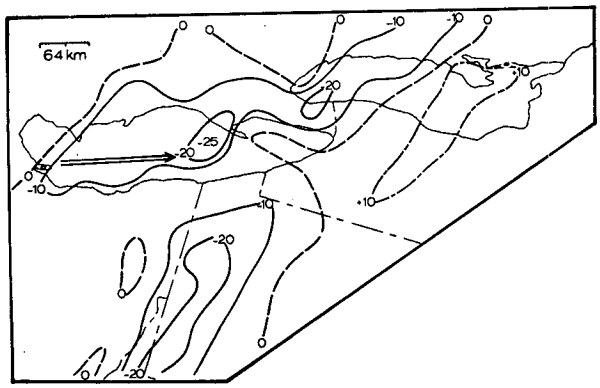

FIG. 6a. 875-mb omegas (μb sec^{-1}) forecast at 6 hr beyond the initialization by the 127-km barotropic model.

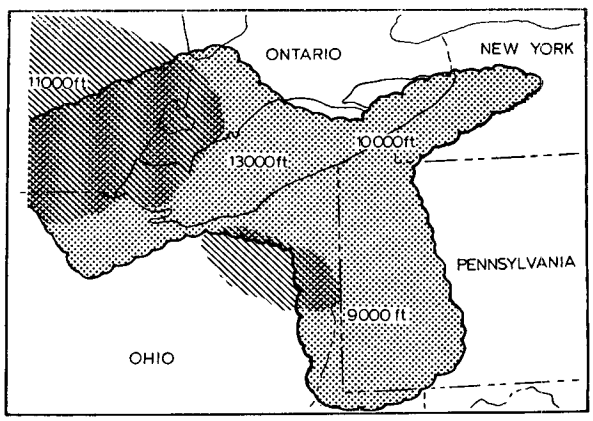

FIG. 6b. WSR-57 (10 cm) radar observations from Buffalo, Pittsburgh and Detroit. Diagonal lines represent echoes at 1745 GMT 4 November, 15 min prior to the barotropic initialization. Stippled portion represents echoes 6 hr later at 2345 GMT 4 November.

the relationship between the forecast gravity wave and observed convection, Fig. 6b illustrates the rapid advance of echoes detected by 10-cm radar during the forecast period. Shading by diagonal lines represents the extent of radar echoes reported by Buffalo, Detroit and Pittsburgh WSR-57 radars 15 min prior to the barotropic initialization. Significant snow shower activity at 1745 GMT 4 November was limited to an area over southeastern lower Michigan. Six hours later, the stippled area shows the rapid spread of convection across most of Lake Erie and its leeward shore, with a broad band of echoes centered along the Ohio-Pennsylvania border. Maximum cloud tops $\geqslant$9000 ft appear only in those regions where forecast ascent extended through the 700-mb surface. In particular, the 9000-ft cloud tops over Pittsburgh are within the mesoscale wavelength feature associated with the forecast convergence field.

The forecast precipitation is shown in Fig. 7 and should be compared with the analyzed values of total snowfall for the period 4–7 November 1967 (Fig. 8). One will note a reasonable correspondence both in intensity and in positioning of the precipitation. Unfortunately, snowfall data were available at only 24-hr increments, preventing a more detailed comparison of snowfall vs time. However, snowfalls $\geqslant$12 inches at Arcade and Westfield, N. Y., lying within the predicted heavy snow area, support the idea that much of the storm total fell during the first day.

A second weaker area of forecast snowfall over eastern Lake Ontario is the result of the interaction of a cold front with the heat island early in the integration. The tendency of the model to position the snowfall two to three grid points west of the analyzed pattern is probably due to the unrealistically rapid fall velocity of particles caused by the 1 level per time step assumption in the numerical model. This amounts to approximately 5–7 m sec^{-1}, or two to three times the velocity of massive rimed or graupel aggregates (Nakaya, 1954).

This snowfall prediction should be compared with that of Lavoie (1972). Using a 6$\times$12 km horizontal mesh, Lavoie was able to generate representative snowfall amounts only after applying upward vertical

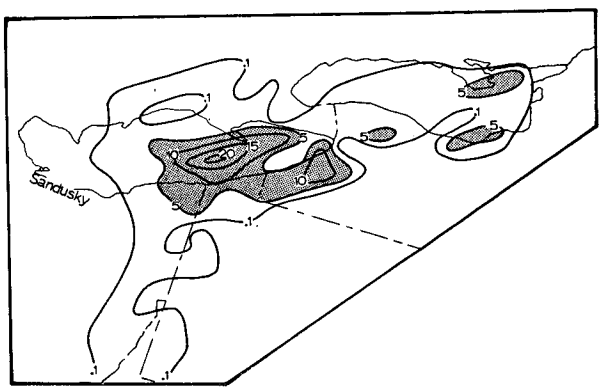

FIG. 7. Six-hour forecast of total snowfall (inches) at 120 time steps from the barotropic initialization at 1800 GMT 4 November. A snowfall-meltwater ratio of 15:1, and an average cloud depth of 3 km over Lake Erie and 1.67 km over Lake Ontario were assumed.

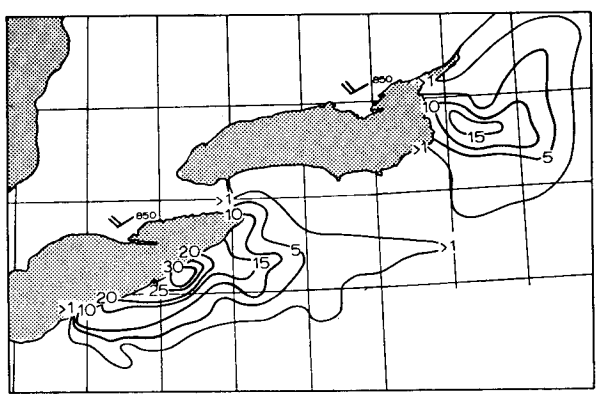

FIG. 8. Total snowfall (inches) for 4–7 November 1967.

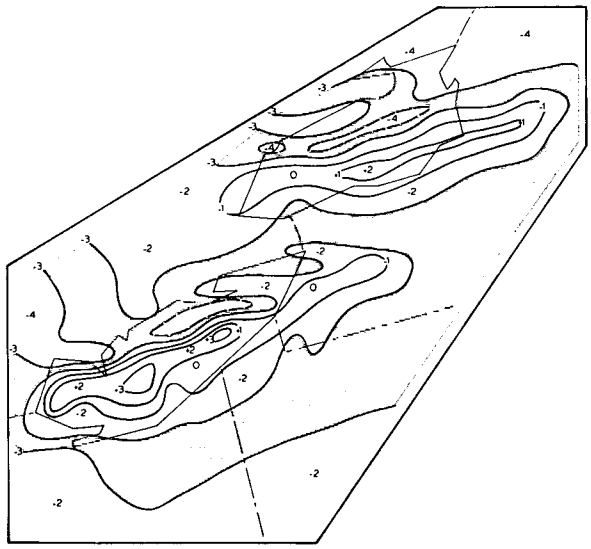

FIG. 9. Six-hour forecast of 950-mb temperature field (°C).

motions achieved after 9 hr of integration for a full 30-hr period. Also, in view of the results presented here showing transient four to six grid-length internal gravity waves, it is questionable whether an assumption of a "steady-state" lake storm is valid over a 24-hr period at the mesoscale.

c. *Ten-level diagnostic omega equation approximation of the initial state*

The final integration was performed with the quasi-geostrophic diagnostic initialization. The integration utilized the initial data from the 0000 GMT 5 November analysis performed in 50-mb increments to the 100-mb level. This initialization is more realistic and should provide the P.E. model with a more vigorous quasi-geostrophic set of forcing functions.

The 32-km P.E. model receives the dependent variables from the 127-km scale by a linear interpolation. The model is then integrated out to approximately 8 hr of real time. Fig. 9 illustrates the 950-mb temperature field predicted after 100 time steps of low-level, lake-induced heat flux and realized latent heating. The maximum temperature increase (from −4C over Lake Erie) of 3–6C should be compared with the results of mesoscale forcing in the absence of synoptic-scale organization shown in Figs. 4b and 5b. The predicted heating is in good agreement with the observations of McVehil and Peace (1966) showing 8C heating in 12 hr for a similar intense lake-effect snowfall.

Additional results indicate patterns of vertical motion, height deformation, and thermal energy input in agreement with the 0745 GMT 5 November radar echoes shown in Fig. 10. For example, the 875-mb omega field seen in Fig. 11 shows a wave-like pattern of ascent over both lakes. Maximum cell tops (11,000 ft)

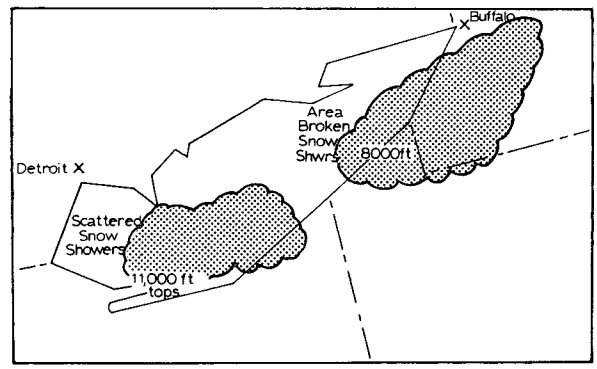

FIG. 10. WSR-57 (10 cm) radar observations at 0745 GMT 5 November corresponding to the approximate 8-hr P.E. forecast.

recorded by WSR-57 10-cm radar are within the predicted $-50\,\mu b\ sec^{-1}$ isopleth. Over eastern Lake Erie, shallow ascent is nearly one order of magnitude weaker where reported maximum cloud tops are 8000 ft. The echo-clear region over extreme northern Lake Erie falls within the region of predicted descent.

It is also important to compare the depth of upward vertical motion shown in Figs. 12a–c over Lakes Erie and Ontario. The entire lower troposphere up to 700 mb is in ascent over southwestern Erie, while the top of upward vertical motion is limited to 800 mb over south-central and southeastern Lake Ontario. This is probably indicative of the residence time of the quasi-geostrophic feature over each lake and the degree to which quasi-geostrophic and lake-induced forcing have combined to release latent heat.

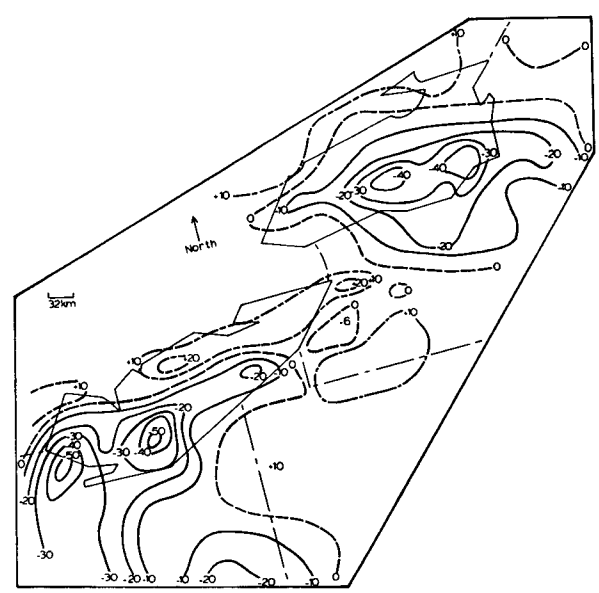

FIG. 11. Eight-hour forecast of 875 mb omega ($\mu b\ sec^{-1}$) at 0742 GMT 5 November 1967. The P.E. forecast was initialized by the 10-level quasi-geostrophic model.

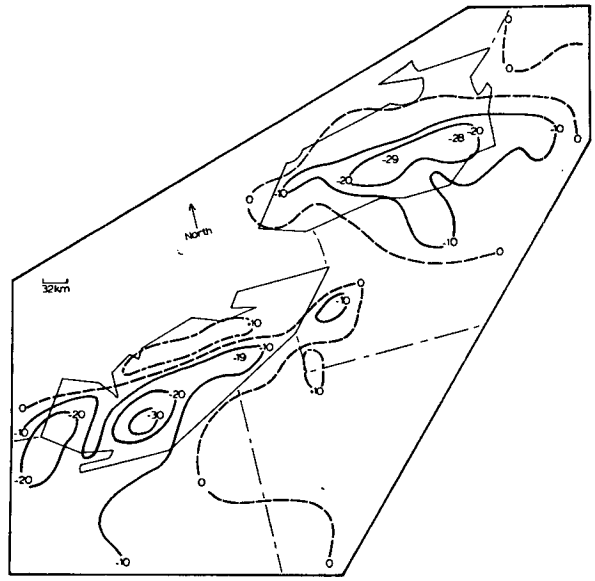

(a)

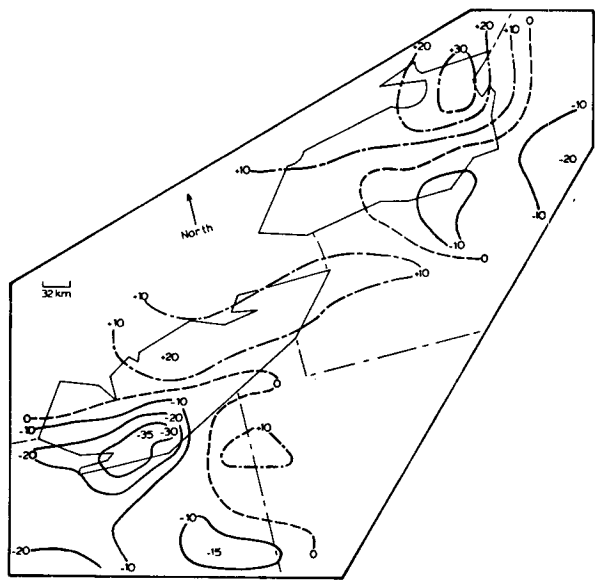

(b)

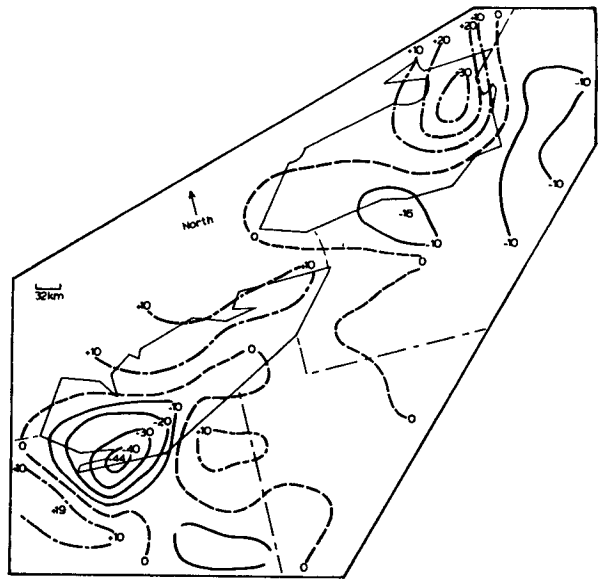

(c)

FIG. 12. Eight-hour forecast of 950-mb (a), 800-mb, (b), and 700-mb (c) omega (μb sec^{-1}) at 0742 GMT 5 November 1967. The P.E. forecast was initialized by the 10-level quasi-geostrophic model.

5. A comparison of results with the 32-km moist P.E. forecast

After 8 hr of integration, the production of vorticity and three-dimensional accelerations has become quite evident. The heating in the lower 50 mb of the atmosphere by an intense vertical energy flux from the warm lakes (~50F) to the cold air (~28F) produced a significant tilt of the geopotential surfaces. This tilt combined with the preexisting tilt of the low-level trough has led to a significant acceleration, horizontal gradient of velocity, convergence, and upward vertical motion field. Once the upward motion has reached sufficient magnitude, the release of latent heat begins to overpower the cooling by adiabatic expansion. This process amplifies the acceleration, convergence and vertical motions.

The degree to which this process has continued may be best understood by noting the omega fields at 875 mb (Fig. 11). The amount to which latent and sensible heating has distorted the flow pattern is most marked over south-central and southwestern Lake Erie. The maximum ascent of more than 50 cm sec^{-1} represents a vertical mass transport more than ten-fold that of typical large-scale atmospheric motions. Significantly, this transformation of the lower troposphere has taken place within 8 hr, or in less time than one radiosonde information span.

Another means of evaluating the significance of these results may be to compare them to the results achieved by other numerical models in relatively similar synoptic situations. For instance, consider the precipitation forecasts realized by the 190-km model of Danard and Rao (1972) and the model developed by Lavoie (1972). Precipitation totals are obtained after longer period forecasts than the nine-level model. The results of the Danard and Rao model lacks horizontal resolution of the mesoscale energy sources on its 190-km grid, and therefore cannot accurately simulate either the configuration or intensity of the vertical motion. The horizontal resolution of Lavoie's model has allowed him to achieve a much finer picture of the vertical motion patterns when compared to the Danard and Rao model. However, the lack of initial synoptic forcing and poor vertical resolution within the model fails to forecast the

intensity of vertical motion and the realistic periodicity in the space-time variation of this quantity.

Paine (1971) has suggested that the internal gravity wave plays an important role in intense atmospheric development. He has presented evidence which shows that this wave form is a means by which the local production of divergence in excess of synoptic-scale values is ducted horizontally. It is reasonable to anticipate, therefore, that such higher frequency modes of atmospheric motion should be an integral part of the simulation presented here. Evidence of such features growing and interacting with the fluid seems especially apparent in the 875-mb omega field where significant latent heat is released.

6. Summary and conclusions

A numerical model has been developed in an effort to link mesoscale with quasi-geostrophic forcing. The model is integrated utilizing several different initial conditions. Results of these integrations indicate a critical role played by latent heating in mesoscale development. The release of latent heat, however, is highly dependent upon preexisting quasi-geostrophic organization. It is seen that gravity waves with wavelengths of approximately four to six grid intervals aid in propagating energy initially realized at smaller scales.

The most successful initialization is that of the quasi-geostrophic diagnostic model. Its ability to simulate mesoscale development depends upon its more realistic description of the vertical variation of the constant pressure surfaces. The intensity and pattern of vertical motions developed by this initialization are superior to those predicted utilizing only mesoscale forcing. In the latter artificial case, only an unrealistic boundary condition or prolonged integrations could produce motions resembling severe lake-effect snowstorms.

Acknowledgments. This study was completed with the support of the Atmospheric Sciences Section, National Science Foundation, under Grant GA-35250. Portions of the research were supported by the Atmospheric Physics and Chemistry Laboratory, NOAA, under Grant E22-49-70.

Also to be acknowledged for generous donation of computer time is the Department of Atmospheric Sciences, State University of New York at Albany. Thanks also go to Robert Duncan, Frank Brown, Bruce Bendini, Joseph Snyder, and all of those employees of the SUNYA computer center facility who gave invaluable assistance in the completion of this work. Ms. Lee and Ms. Grey typed the manuscript.

APPENDIX A

List of Symbols

C_1, C_2	low-level moisture flux, condensation functions
C_d	drag coefficient
C_{pm}	specific heat for moist air at constant pressure
f	Coriolis parameter
f_0	constant value of f
$f(x)$	function of variable x
F_x, F_y	frictional stresses
g	gravitational acceleration
H	scale height
H_1	low-level turbulent flux of sensible heat
H_2	latent heating
J	Jacobian operator
L	latent heating
m	map scale factor
p, P	pressure
P_{300}, P_{950}	pressure surfaces
P_s	surface pressure
P.E.	primitive equation
Q	mixing ratio
Q_{sat}	saturation mixing ratio
T	temperature
T_v	virtual temperature
u, v	horizontal wind components
$\mathbf{V}$	total velocity vector
$\mathbf{V}_s$	surface velocity vector
$\mathbf{V}\cdot\nabla$	advection
w	vertical velocity in z system
Z	height of pressure surface
∇	del, gradient operator
∇^2	Laplacian operator
$\nabla\cdot\mathbf{V}$	divergence
Δ	delta, finite increment in space or time
$\Delta t, \Delta X$	increments in time and X
Δc	condensate
ϵ	dependent variable
$\partial/\partial x, \partial/\partial y$	horizontal space derivative
$\partial/\partial t$	local derivative with respect to time
$\partial/\partial P$	local derivative with respect to pressure
$\partial/\partial z$	local derivative with respect to height
ζ	relative vorticity
Φ	geopotential
ω	vertical velocity $(\partial P/\partial t)$ in pressure system
σ	static stability

APPENDIX B

Cumulus Parameterization Scheme

If X is any grid point, then the requirements for adding non-hydrostatic latent heating are

1) X_{IJK}, X_{I+1JK}, X_{I-1JK}, X_{IJ+1K}, X_{IJ-1K}, X_{IJK+1}, and X_{IJK-1} are all saturated.
2) Above these seven grid points we have a mean ω equal to $-20\,\mu$b sec^{-1}.
3) The temperature decreases from X_{IJK-1} to X_{IJK+1}.

We assume 30% of the grid box contains convection, where 10% of the grid box has omegas ≈ 10 times the 32-km omega, and 20% has omegas ≈ 5 times the 32-km omega. Upon defining

$$H_{\text{total } L} \approx 2\frac{\omega_{\text{total}}}{\omega_{\text{threshold}}} H_{32 \text{ km } L} + H_{32 \text{ km } L},$$

then

$$\omega_{\text{total}} = \omega_{I+1JK} + \omega_{I-1JK} + \omega_{IJ+1K} + \omega_{IJ-1K} + \omega_{IJK+1} + \omega_{IJK-1} + \omega_{IJK},$$

where $\omega_{\text{threshold}} = -140\ \mu\text{b sec}^{-1}$ or (7 times $-20\ \mu\text{b sec}^{-1}$) and $H_{32 \text{ km}L}$ is the latent heating at 32 km.

REFERENCES

Danard, M. B., and G. V. Rao, 1972: Numerical study of the effects of the Great Lakes on a winter cyclone. *Mon. Wea. Rev.*, **100**, 374–382.

Gerrity, J. P., and R. D. McPherson, 1970: Noise analysis of a limited-area fine mesh prediction model. ESSA Tech. Memo. WBTM NMC 46, 81 pp.

Jiusto, J. E., and M. L. Kaplan, 1972: Snowfall from lake-effect storms. *Mon. Wea. Rev.*, **100**, 62–66.

Kaplan, M. L., and D. A. Paine, 1972: A macroscale-mesoscale numerical model of intense baroclinic development. *J. Appl. Meteor.*, **11**, 1224–1235.

Lavoie, R. L., 1968: A mesoscale numerical model and lake effect storms. Ph.D. thesis, Pennsylvania State University, 102 pp.

——, 1972: A mesoscale numerical model of lake-effect snowstorms. *J. Atmos. Sci.*, **29**, 1025–1040.

Matsuno, T., 1966: Numerical integrations of the primitive equations by a simulated backward difference method. *J. Meteor. Soc. Japan*, **44**, 76–83.

McPherson, R. D., 1971: Recent research into numerical methods at the National Meteorological Center. NOAA Tech. Memo. NWS NMC-50, 35 pp.

McVehil, G. E., and R. L. Peace, 1966: Project lake effect, a study of lake effect snowstorms. Rept. VC-2142-P-2, Cornell Aeronautical Laboratory 52 pp.

Nakaya, U., 1954: *Snow Crystals, Natural and Artificial*. Harvard University Press, 510 pp.

Nitta, T., 1962: The outflow boundary condition in numerical time integration of advective equations. *J. Meteor. Soc. Japan*, **40**, 13–24.

Paine, D. A., 1971: The diagnosis and prediction of synoptic scale influences leading to mesoscale lake-effect development. Ph.D. thesis, State University of New York at Albany, 95 pp.

——, and M. L. Kaplan, 1971: The linking of multiscaled energy sources creating a severe local winter storm. *Preprints Seventh Conf. Severe Local Storms*, Amer. Meteor. Soc., 299–306.